BNL-213562-2020-JAAM

Quinary Defect-rich Ultrathin Bimetal Hydroxide Nanosheets for Water Oxidation

Z. Liu, X. Tong

To be published in "ACS Applied Materials & Interfaces"

November 2019

Center for Functional Nanomaterials

Brookhaven National Laboratory

U.S. Department of Energy

USDOE Office of Science (SC), Fusion Energy Sciences (FES) (SC-24)

Notice: This manuscript has been authored by employees of Brookhaven Science Associates, LLC under Contract No. DE-SC0012704 with the U.S. Department of Energy. The publisher by accepting the manuscript for publication acknowledges that the United States Government retains a non-exclusive, paid-up, irrevocable, world-wide license to publish or reproduce the published form of this manuscript, or allow others to do so, for United States Government purposes.

DISCLAIMER

This report was prepared as an account of work sponsored by an agency of the United States Government. Neither the United States Government nor any agency thereof, nor any of their employees, nor any of their contractors, subcontractors, or their employees, makes any warranty, express or implied, or assumes any legal liability or responsibility for the accuracy, completeness, or any third party's use or the results of such use of any information, apparatus, product, or process disclosed, or represents that its use would not infringe privately owned rights. Reference herein to any specific commercial product, process, or service by trade name, trademark, manufacturer, or otherwise, does not necessarily constitute or imply its endorsement, recommendation, or favoring by the United States Government or any agency thereof or its contractors or subcontractors. The views and opinions of authors expressed herein do not necessarily state or reflect those of the United States Government or any agency thereof.

Quinary Defect-rich Ultrathin Bimetal Hydroxide Nanosheets for Water Oxidation

Zhijuan Liu,[a,b] Yu-cheng Huang,[c] Yanyong Wang,[a] Jiajie Cen,[b] Haotian Yang,[b] Xiaobo Chen,[b] Xiao Tong,[b] Dong Su,[b] Chung-Li Dong[c*] and Shuangyin Wang[a*]*

[a] State Key Laboratory of Chem/Bio-sensing and Chemometrics, College of Chemistry and Chemical Engineering, Hunan University, Changsha, 410082, China.

[b] Center for Functional Nanomaterials, Brookhaven National Laboratory, Upton, New York, 11973, United States.

[c] Department of Physics, Tamkang University, Tamsui, 251, Taiwan.

KEYWORDS: Quinary bimetal hydroxide nanosheets; exfoliation; *in-situ* S, F co-filling; vacanies; electrochemical water oxidation

ABSTRACT: Electronic structure of layered double hydroxides (LDHs) can be modulated by heteroatom-doping and creating vacancies. The number of exposed active sites can be enriched by exfoliating bulk structure into fewer layers. Herein, we successfully achieved multielement-doping and exfoliation for Co_3Fe LDHs by one SF_6-plasma etching step at room temperature (named as Co_3Fe LDHs-SF_6). The obtained Co_3Fe LDHs-SF_6 ultrathin nanosheets display outstanding oxygen evolution reaction (OER) activity, which only needs 268 mV overpotential to reach 10 mA cm^{-2}. Tafel slope and charge transfer resistance are dramatically decreased indicating faster reaction kinetic rate. The excellent OER activity can be attributed to increased number of active sites and optimized electronic structure modulated by the incorporation of

electron-withdrawing F, electron-donating S and abundant vacancies resulting in proper adsorption energy to oxygen species.

INTRODUCTION

OER, whose reaction pathway is thermodynamically unfavorable, seriously hinders putting metal-air batteries[1] and water splitting devices[2, 3] into market. Transition metal compounds have attracted much interest to replace noble RuO_2 and IrO_2 as efficient OER electrocatalysts because of their rich resources, cheap cost and preferable electrochemical activity. LDHs, whose component and interlamellar distance can be tunable, have been extensively explored as efficient OER electrocatalysts.[4]

In alkaline solution, OER process involves the adsorption of OH^-, formation of O_2 and desorption of O_2.[5] The adsorption energy of active sites and oxygen-containing species at each step has a significant effect on OER activity. High or low adsorption energy can lead to strong or weak adsorption of reaction intermediates, which is not beneficial for reaction occurring.[6] Increasing the number of active sites and improving intrinsic activity are two effective strategies to enhance catalytic activity of catalysts.[7] Hierarchical structure with various morphology e.g. nanocubes,[8] nanoflowers[9] or nanowires[10] has been designed to expose more active sites to participate in electrochemical reaction. For LDHs, exfoliation of bulk LDHs into monolayer or fewer layers can dramatically increase exposed active sites to facilitate electrocatalytic process.[11] Heteroatom-doping is a valid method to improve electrocatalysts' intrinsic activity.[12] Recently, N-doped metal-free carbon nanomaterials displays charming oxygen reduction reaction (ORR) activity compared to commercial Pt/C because of broken electroneutrality resulting from stronger electronegativity of N than C leading to high ORR activity.[13] B-doping, whose

electronegativity is lower than C, also can increase ORR activity of carbon nanomaterials because of producing positively charged B atoms as active sites. When B and N with opposite property are co-doped into carbon, asymmetric charge density would be offset but increased asymmetric spin density of carbon atom processed proper adsorption energy to reaction intermediates leads to much higher ORR activity than B or N doped carbon.[14] For transition metal electrocatalysts, metal sites often are regarded as active sites.[15] Tuning adjacent anion atoms around metal sites can effectively modulate electronic structure to form an optimized adsorption configuration to oxygen-containing species.[16]

F, which processes higher electronegativity (4.0) compared with O (3.5), can significantly tune electronic structure of metal hydroxide. Jiang et.al reported F-doped Ni hydroxyl oxide exhibited outstanding OER activity. The incorporation of F^- can increase surface polarity, hydrophilic and content of Ni^{3+} resulting in decreased adsorption energy to reactive oxygen intermediate.[17] Zhang et.al reported that too positive electronic field of metal ions would be adverse to desorption of oxygen species, which limits the occurrence of next elementary reactions.[6] By regulating anions atomic ratio of polarized S (2.5) and nonpolarized O, the electronic structure of NiFe (oxy)sulfides can be optimized and OER process is promoted. With the co-incorporation of electron-withdrawing F and electron-donating S, the electron distribution of LDHs would be significantly adjusted leading to superior OER activity. Creating vacancies (oxygen vacancies and metal vacancies) is also an effective method to modify intrinsic activity of electrocatalysts.[18,19] These unsaturated coordinated sites often optimize the adsorption energy to reaction intermediates and exhibit charming catalytic activity.[20,21] Set all these merits in one, it's desirable to develop electrocatalysts with numerous active sites, multielement-doping and rich

vacancies.

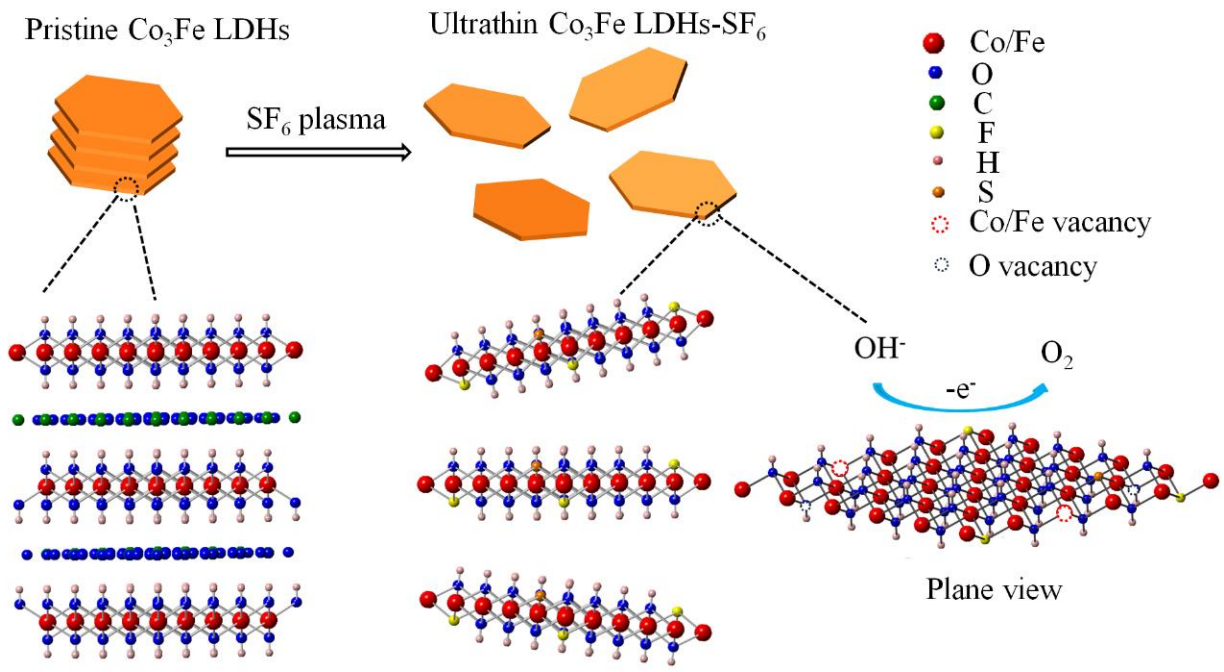

Scheme 1. Schematic illustration of preparation of Co_3Fe LDHs-SF_6.

Herein, we successfully synthesized S, F co-doping Co_3Fe LDHs nanosheets with oxygen vacancies and metal vacancies by one step at room temperature (Scheme 1). With SF_6-plasma treatment, pristine bulk Co_3Fe LDHs can be exfoliated into fewer layers to expose more active sites. Moreover, ionized SF_6-plasma can create oxygen vacancies and metal vacancies at LDHs surface and achieve *in-situ* S, F co-filling into part of oxygen vacancies. Co_3Fe LDHs-SF_6 exhibits superior OER activity, which only needs overpotential of 268 mV to reach 10 mA cm^{-2}. The outstanding electrochemical property can be attributed to more active sites participated in OER owing to increased surface area and optimized electronic structure with the filling of S, F into part oxygen vacancies and creating of vacancies. This work not only provides a one-step method to achieve exfoliation, multielement-doping and creating vacancies at room temperature

but also gives a deep insight into the relationship between electronic structure and electrocatalytic activity.

RESULT AND DISCUSSION

Morphology of electrocatalysts

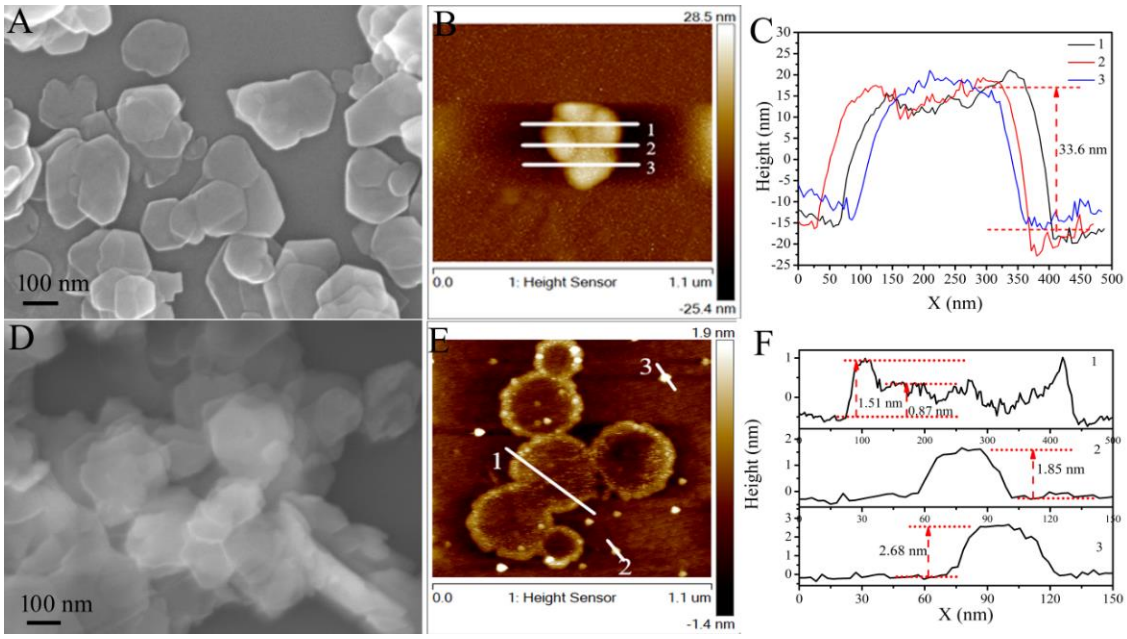

Figure 1. SEM images (A, D), AFM images (B, E) and height carves (C, F) of pristine Co_3Fe LDHs and Co_3Fe LDHs-SF_6, respectively.

Bulk LDHs usually exhibit poor OER activity because of limited exposed active sites and poor electronic conductivity. To maximize the number of active sites and improve intrinsic activity, the strategy of exfoliating bulk LDHs into less layered nanosheets has been generally applied.[22] In order to explore the morphology, size and thickness evolution of LDHs nanosheets, Scanning electron microscope (SEM) and atomic force microscope (AFM) analysis were performed. As shown in Figure 1A-C, the size of pristine Co_3Fe LDHs nanosheets is about 100-300 nm and the thickness is about 33.6 nm. After treated by SF_6-plasma for 80 s, Co_3Fe LDHs-SF_6 nanosheets

become thin and transparent displayed in Figure 1D. The size of Co_3Fe LDHs-SF_6 nanosheets is about 50-300 nm. The decreased size may be attributed to etching function of SF_6-plasma. The thickness of Co_3Fe LDHs-SF_6 nanosheets is about 0.87-2.68 nm indicating the effective exfoliation of pristine Co_3Fe LDHs into fewer layers (Figure 1E, F). Pristine Co_3Fe LDHs were also suffered from different SF_6-plasma treatment time to investigate exfoliation progress as shown in Figure S1-5. The nanosheets become much thinner and more transparent with increase of SF_6-plasma treatment time.

Crystalline phase structure of electrocatalysts

To explore crystalline phase evolution of LDHs after SF_6-plasma treatment, Powder X-ray diffraction (XRD) and transmission electron microscopy (TEM) analysis were carried on. As shown in Figure 2A, XRD pattern of pristine Co_3Fe LDHs is consistent with PDF#50-0235 indicating the successful synthesis of LDHs. As shown in Figure S6, the TEM image displays nanosheets morphology and its selected area electron diffraction (SAED) patterns can be indexed to (0 1 2) and (1 1 3) planes of LDHs. The lattice fringe of 0.255 nm in high-resolution TEM (HRTEM) (Figure 2B) can be attributed to (0 0 9) plane of LDHs. However, the diffraction peaks of Co_3Fe LDHs-SF_6 disappeared as shown in Figure 2A indicating effective exfoliation of LDHs. Nanosheets morphology and LDHs phase structure are still kept according to Figure S7. The lattice fringe displayed in HRTEM (Figure 2C) is still 0.255 nm. Based on above, pristine Co_3Fe LDHs have been successfully exfoliated but still kept origin phase structure. F and S have been successfully introduced after SF_6-plasma treatment as shown in Figure S8. Co, Fe, O, F and S are distributed uniformly in Co_3Fe LDHs-SF_6 in Figure 2D-J, which is consistent with energy dispersive spectrometer (EDS) mapping data as shown in Figure S9.

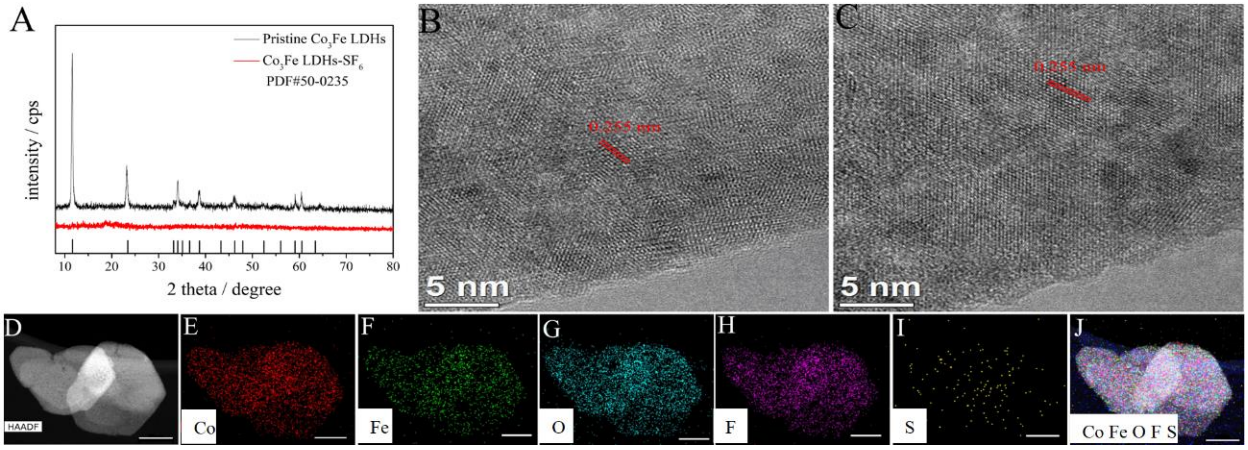

Figure 2. (A) XRD pattern of pristine Co_3Fe LDHs and Co_3Fe LDHs-SF_6. HRTEM image of pristine Co_3Fe LDHs (B) and Co_3Fe LDHs-SF_6 (C) STEM-mapping images (D-J) of Co_3Fe LDHs-SF_6.

Electronic structure and coordination configuration of electrocatalysts

X-ray photoelectron spectroscopy (XPS) and X-ray adsorption spectroscopy (XAS) technique were performed to explore electronic structure and coordination configuration of pristine Co_3Fe LDHs and Co_3Fe LDHs-SF_6. In Figure S10, the peaks of F 1s and S 2p can be clearly observed in Co_3Fe LDHs-SF_6 compared with pristine Co_3Fe LDHs indicating successful doping of F and S. The relative contents of Co, Fe, O, C, F and S are summarized in Table S1. The ratio of Co/Fe still is kept about 3:1, which is also consistent with inductively coupled plasma optical emission spectrometer (ICP-OES) data shown in Table S2. For Co 2p, the peak of Co $2p_{3/2}$ shifts to lower binding energy suggesting the production of Co^{3+} (Figure S11A). Meanwhile, the peak of Fe $2p_{3/2}$ shifts to higher binding energy indicating increased valance state of iron (Figure S11B). For O 1s, high-resolution XPS analysis was performed to get a deep understanding in detail. As shown in Figure S11C, O 1s can be divided into three peaks. The peaks at 530.2 eV and 532.3 eV are attributed to metal-oxygen bond and adsorbed oxygen at surface, respectively. Meanwhile the peak at 531.65 eV is corresponded to oxygen vacancies.[23] The relative content of oxygen vacancies in pristine Co_3Fe LDHs and Co_3Fe LDHs-SF_6 is summarized in Tables S3. It's

obvious to see more oxygen vacancies could be produced after plasma treatment. For C 1s, the peak at about 289.9 eV in Co_3Fe LDHs-SF_6 attributed to carbonate species is decreased significantly compared with pristine Co_3Fe LDHs, which can indicate the exfoliation of LDHs by removing intercalated carbonate.[24] The main peak of F 1s is about at 684.8 eV, which confirms the formation of metal-fluorine bond.[25] Meanwhile, the peak of S 2p at about 169.5 eV corresponds to oxidized sulfur species, which may be resulted from oxidation of metal-sulfur bond exposed to air.[26] From XPS analysis, it can be concluded that F and S have been successfully incorporated into LDHs, numerous vacancies have been produced and finally electronic structure has been effectively modulated. X-ray absorption spectroscopy (XAS) has been used to explore subtle electronic and geometrical structure of LDHs. The metal 2p→3d L pre-edge transition is electric dipole allowed and processes high intensity, which can provide more detailed information about electronic structure. The L-edge spectra of transition metal is originated from dipole allowed 2p→3d transition and comprised with two edge, L_2 and L_3, because of spin-orbit splitting of the $2p_{3/2}$ and $2p_{1/2}$ orbital. Careful analysis of relative intensities of the L_3 and L_2 peaks can provide useful information about valance state of metal atom.[27] Figure 3A displays Co L-edge spectra, where L_3 and L_2 are located at around 776 eV and 792 eV energy position, respectively. After plasma treatment, qualitative information about the relative intensity ratio of L_3/L_2 is decreased can be observed, which indicates lower electron occupancy in the d orbital.[27] Co L_3-edge is split into two traits and the increased ratio of high energy/low energy indicating increased oxidation state of Co.[28, 29] For Fe L-edge, L_3 and L_2 edge are located at 709 eV and 723 eV, respectively, displayed in Figure 3B. L_3-edge always followed by a pre-edge in both pristine Co_3Fe LDHs and Co_3Fe LDHs-SF_6 indicating the oxidation state of iron mainly is trivalent.[30] Inset image of Figure 3B shows the shift of Fe L_3-edge to higher energy, which can

be deduced that the valance state of iron is increased after plasma treatment.[31] Figure 3C provides information about O k-edge spectra, which is made up of two characteristic parts. The first feature of pre-edge at region about 530 eV is attributed to energy transition from O 1s to hybridized metal 3d-O 2p orbital. The second broad band at about 542 eV is attributed to orbital hybridization of O 2p and metal 4 sp. The pre-edge of O K-edge in Co_3Fe LDHs-SF_6 shifts to lower energy and intensity of broad band is enhanced, which all can be corresponded to oxidation of metal ions.[32,33] X-ray absorption near edge structure (XANES), at low energy part of XAS spectra, is composed with pre-edge and edge. The pre-edge, which is originated from electric dipoleforbidden 1s→3d transition and can become electric quadrupole allowed through 3d and 4p hybridization, is sensitive to metal coordination configuration and symmetry. The edge is originated from 1s→4p dipole-allowed transition and edge energy can be indicative of valance state of metal.[34] As shown in Figure 3D, for Co *K*-edge the main adsorption edge of Co_3Fe LDHs-SF_6 is enhanced, which can be attributed to more unoccupied Co 4p states with the incorporation of much F with strong electronegativity. The inset image displays the absorption edge was shifted to higher energy of Co_3Fe LDHs-SF_6 indicating increased oxidation state of cobalt, which is consistent with XPS results. A similar phenomenon has been observed for Fe K-edge indicating the electronic environment of metal sites has been dramatically modulated after plasma treatment. Extended x-ray absorption fine structure spectroscopy (EXAFs) was used to determine the local coordination configuration of active sites. Figure S12A and B present Co and Fe K-edge $k^3\chi(k)$ EXAFs oscillation carves. Similar oscillation can indicate all MO_6 octahedron-liked atomic configurations in Co_3Fe LDHs-SF_6 and pristine Co_3Fe LDHs. As shown in Figure 3F and G, two primary Fourier-transformed peaks are presented in metal R-space. The first peak at around 1.6 Å can be assigned to first coordination shell of metal-O bond and the second peak

at around 2.6 Å are attributable to second coordination shell of metal-metal bond.[35] Numerous metal vacancies are produced after SF_6-plasma treatment, which can be concluded from an obvious decreased intensity of second peaks. The intensity of first peak also exhibits a little decrease and it can be deduced the existence of oxygen vacancies.[24] What's surprise, plasma technique has been extensively applied to develop oxygen vacancy at metal oxide surface.[36] So, the little changed intensity of first peak can be owing to filling of oxygen vacancies with S and F ions.[37] Above all, the electronic structure of Co_3Fe LDHs nanosheets has been effectively modulated after SF_6-plasma treatment. Much vacancies (metal vacancies and oxygen vacancies) and heteroatom-doping (S and F) have been successfully *in-situ* achieved by one step with SF_6-plasma etching. It has been reported by Xie et.al that when the thickness of nanomaterials reduced to atomic scale, Co^{3+} spin state would change from low spin ($t_{2g}^6e_g^0$) to high spin ($t_{2g}^4e_g^2$). High spin Co^{3+} octahedron will distort owing to Jahn–Teller effect to form lower energy system facilitating OER process.[38] F-doping, whose electronegativity is higher than O, can increase iconicity of metal-oxygen bond, hydrophily in water solution and oxidation state of metal ions resulting in optimized adsorption energy to reaction intermediates.[39] Too strong positive electric field of metal sites will be unfavorable to desorption of oxygen species. With the further incorporation of S, which has lower electronegativity compared with O, the adsorption and desorption energy to oxygen-containing intermediates would be regulated to a suitable value. Co_3Fe LDHs-SF_6 is expected to exhibit excellent OER activity.

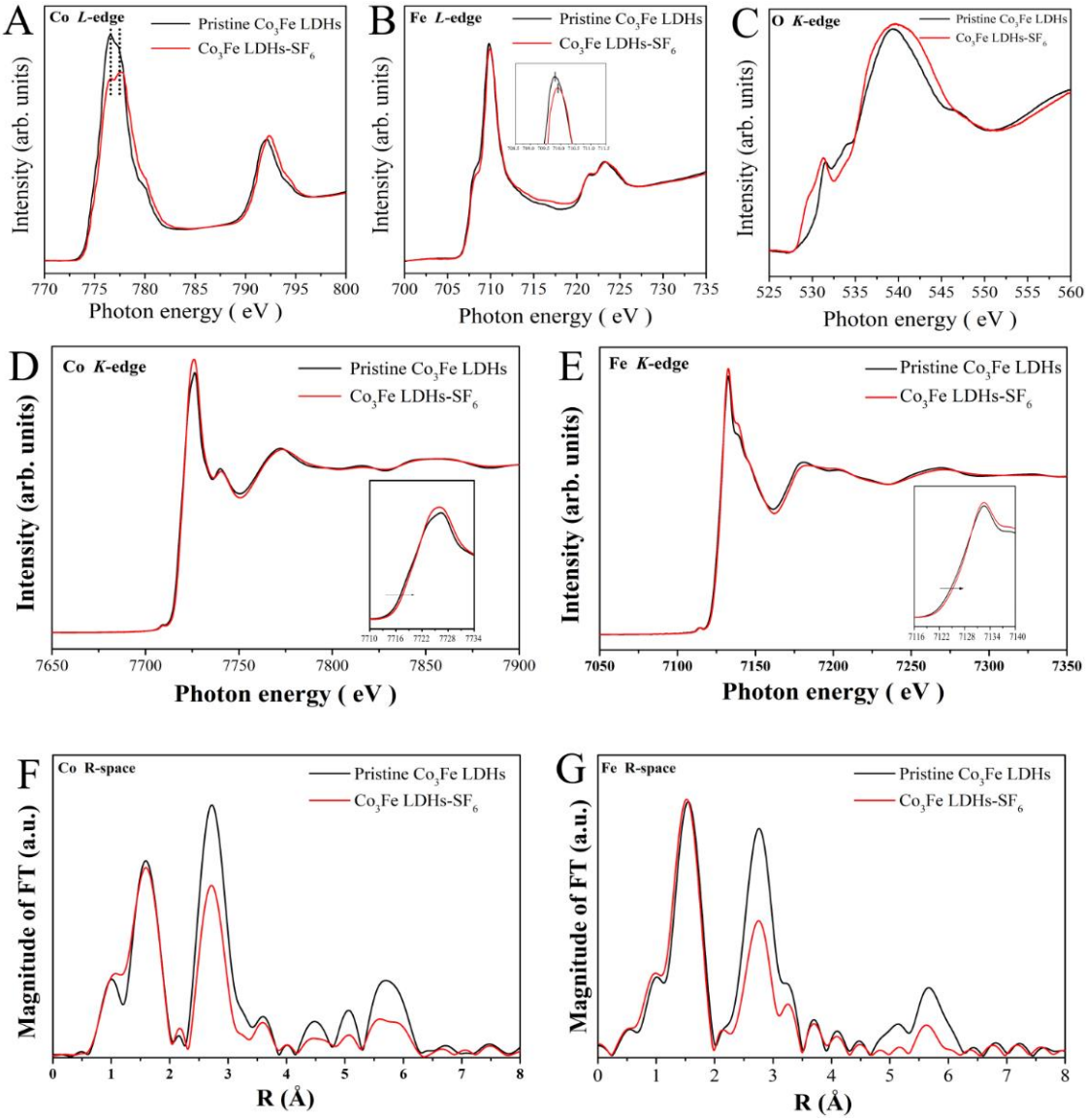

Figure 3. XAS of Co L-edge (A), Fe L-edge (B) and O K-edge (C); XANES of Co K-edge (D) and Fe K-edge (E); FT-EXAFS of Co-K edge (F) and Fe-K edge (G) for pristine Co_3Fe LDHs and Co_3Fe LDHs-SF_6. Inset image in B is enlarged L_3 peak of Fe; Inset image in D and E show the main edge region of pristine Co_3Fe LDHs and Co_3Fe LDHs-SF_6, respectively.

Outstanding electrocatalytic property

With the incorporation of S, F and rich unsaturated coordination sites, Co_3Fe LDHs-SF_6 is expected to exhibit outstanding electrocatalytic activity. A three-electrode system was used to

evaluate OER activity of pristine Co_3Fe LDHs and Co_3Fe LDHs-SF_6. As shown in Figure 4A, Co_3Fe LDHs-SF_6 exhibits more excellent electrocatalytic activity than pristine Co_3Fe LDHs. The overpotential at current density of 10 mA cm^{-2} for Co_3Fe LDHs-SF_6 is 268 mV, which is 53 mV less than pristine Co_3Fe LDHs (321 mV). In Figure 4B, Tafel slope of pristine Co_3Fe LDHs is 62.28 mV/dec while that of Co_3Fe LDHs-SF_6 is 40.12 mV/dec, indicating faster reaction kinetics of Co_3Fe LDHs-SF_6. As displayed in Figure 4C, to reach 20 mA cm^{-2}, Co_3Fe LDHs-SF_6 only needs an overpotential of 279 mV while 350 mV is needed for pristine Co_3Fe LDHs. Meanwhile, Co_3Fe LDHs-SF_6 can obtain a current density of 35.04 mA cm^{-2} while pristine Co_3Fe LDHs merely can reach 3.48 mA cm^{-2} at 1.52 V. All of above demonstrate that Co_3Fe LDHs-SF_6 exhibits outstanding electrocatalytic activity. OER activity of Co_3Fe LDHs that have been suffered by different SF_6-plasma treatment time has been evaluated to explore the best treatment condition. It can be seen from Figure S13 that Co_3Fe LDHs that treated by SF_6-plasma for 80 s could exhibit the most outstanding OER activity. Electrochemical impedance spectroscopy (EIS) was further used to understand reaction kinetic rate under OER process. As displayed in Figure 4D, Co_3Fe LDHs-SF_6 exhibits smaller charge transfer resistance (R_{ct}) than pristine Co_3Fe LDHs. Nyquist plots were modeled by equivalent circuit in Figure S14. The ohmic resistance (R_Ω) is 7.89 Ω and R_{ct} is 8.98 Ω for Co_3Fe LDHs-SF_6, which is much smaller than pristine Co_3Fe LDHs, whose R_Ω is 12 Ω and R_{ct} is 61.5 Ω. The smaller R_Ω of Co_3Fe LDHs-SF_6 indicates good electronic conductivity of Co_3Fe LDHs-SF_6. Ultraviolet-visible spectroscopy (UV-vis) study was also carried out to determine the band gap of pristine Co_3Fe LDHs and Co_3Fe LDHs-SF_6. As shown in Figure S15, the band gap of Co_3Fe LDHs-SF_6 is obviously smaller than pristine Co_3Fe LDHs, which also demonstrates good electronconductivity of Co_3Fe LDHs-SF_6.[40] In order to explore the effect of oxygen vacancy, metal vacancy and S,F co-filling separately, Co_3Fe LDHs

with only oxygen vacancy (Co_3Fe LDHs-V_O), only metal vacancy (Co_3Fe LDHs-V_M), only S-filling (Co_3Fe LDHs-S) and only F-filling (Co_3Fe LDHs-F) were designed and synthesized. As shown in Figure S16, with the incorporation of oxygen vacancy, metal vacancy, S-filling into oxygen vacancy with metal vacancy and F-filling into oxygen vacancy with metal vacancy, respectively, the electrochemical performance of Co_3Fe LDHs all can be enhanced. Co_3Fe LDHs-SF_6 exhibits better electrochemical performance than Co_3Fe LDHs-S and Co_3Fe LDHs-F, which demonstrates the synergy effect of S and F leading to outstanding electrochemical capacity of Co_3Fe LDHs-SF_6. Durability is also an important index for electrocatalysts. As shown in Figure 4E, the electrocatalytic activity of Co_3Fe LDHs-SF_6 declines a little after 2000 CV cycles indicating preferable stability. Cyclic voltammetry (CV) carves were also recorded to calculated double layer capacitance (C_{dl}) in Figure S17. The C_{dl} of Co_3Fe LDHs-SF_6 is 42.22 mF/cm^2, which is about 1.65 times larger than pristine Co_3Fe LDHs, indicating increased electrochemical active surface areas (ECSA) after SF_6-plasma treatment. Normalized by ECSA, Co_3Fe LDHs-SF_6 still exhibits more excellent OER activity than pristine Co_3Fe LDHs (Figure S18), which demonstrates improved intrinsic activity. Brunauer–Emmett–Teller (BET) analysis was also carried on to evaluate increased number of active sites resulting from exfoliation. As displayed in Figure S19, Co_3Fe LDHs–SF_6 processes much larger specific surface area (50.11 cm^2 g^{-1}) than pristine Co_3Fe LDHs (15.64 cm^2 g^{-1}). Co_3Fe LDHs–SF_6 also exhibits better electrochemical activity than pristine Co_3Fe LDHs when normalized by BET demonstrating enhanced intrinsic activity after exfoliation (Figure S20). Compared with some highly active electrocatalysts, Co_3Fe LDHs-SF_6 also processes promising electrocatalytic activity (Figure 4F and Table S4).

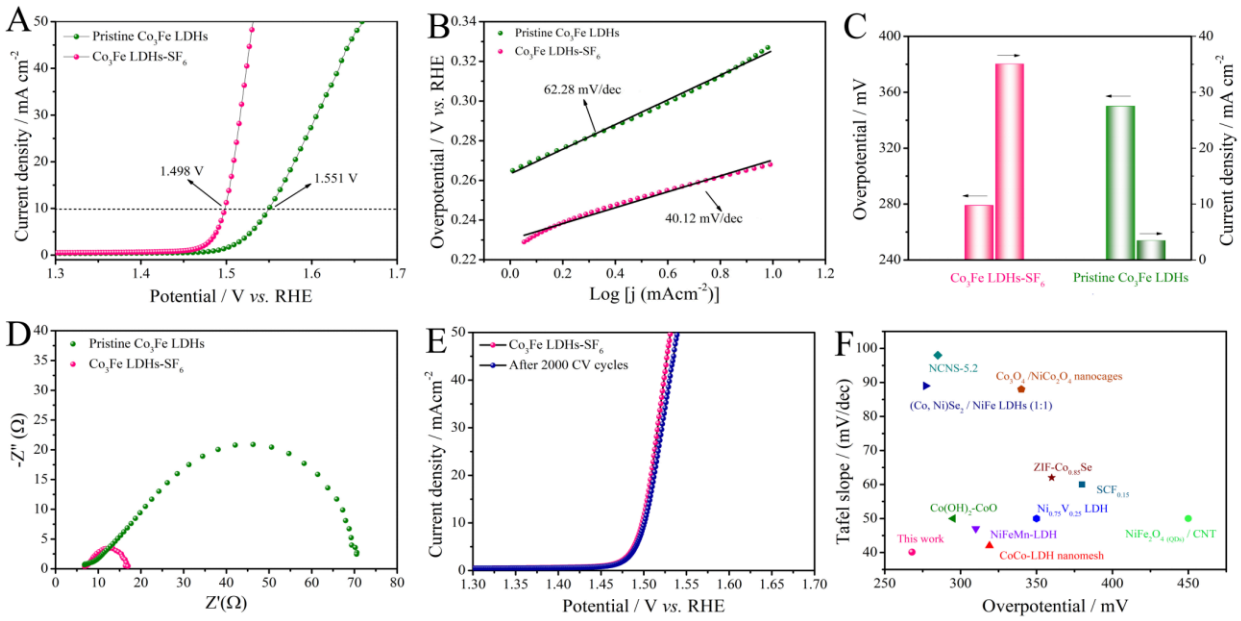

Figure 4. LSV carves for OER of pristine Co_3Fe LDHs and Co_3Fe LDHs-SF_6; (B) the corresponding Tafel plots; (C) Overpotential at current density of 20 mA cm^{-2} and current density at 1.52 V; (D) EIS plots of pristine Co_3Fe LDHs and Co_3Fe LDHs-SF_6 at 1.51 V; (E) Durability test of Co_3Fe LDHs-SF_6 after 2000 CV cycles; (F) Comparing the overpotential at 10 mA cm^{-2} and Tafel slope with some highly active OER catalysts in 1.0 M KOH.

Post-characterization after stability test

To explore structure evolution of Co_3Fe LDHs-SF_6 after stability test, XPS was performed. As shown in Figure S21, peaks of F 1s and S 2p still were kept after durability test. The relative content of Co, Fe, O, C, F and S was summarized in Table S5. The peak of Co 2p was shifted to lower binding energy and the peak of Fe 2p was shifted to higher binding energy, which indicates increased valance state of Co and Fe under oxidative condition during OER process (Figure 5A and B). For O 1s spectra of Co_3Fe LDHs-SF_6 after 2000 CV cycles (Figure 5C), it can be divided into three peaks. The peak at 531.60 eV, 530.95 eV and 529.4 eV are attributed to adsorbed oxygen at surface, oxygen vacancies and metal-oxygen bond, respectively. Compared with Co_3Fe LDHs-SF_6, peaks of O 1s are all shift to lower bonding energy, which could be due

to the dissociation of metal-fluoride bond at electrocatalyst surface.[25] In order to detect the dissolution of Co and Fe after stability test of Co_3Fe LDHs-SF_6, inductively coupled plasma-optical emission spectrometry (ICP-OES) was carried out. As shown in Table S7, Co and Fe were detected and the concentration of Co and Fe was 0.16 and 1.42 mg/L, respectively, corresponding to 0.28 (wt)% and 2.4 (wt)% loss of Co_3Fe LDHs-SF_6 after stability test. The relative content of oxygen vacancy and metal-oxygen bond are summarized in Table S6. The content of oxygen vacancy is decreased but the content of metal-oxygen bond is increased after durability test. It can be deduced that metal hydroxide was formed at surface because of high potential for OER in alkaline solution.[7] The peaks of F 1s and S 1s (Figure 5D and E) also display a shift to lower binding energy after SF_6-plasma treatment, which can be attributed to oxidation of F ions at surface with a little remain. As shown in Figure 5F, the feature of carbonate species becomes obvious after durability test, which might be caused by carbonate derived from dissolution of CO_2 from air in KOH intercalate LDHs nanosheets.[41] Based on above, a metal hydroxide layer would be formed at the surface of Co_3Fe LDHs-SF_6 during OER process and worked as active sites for OER.

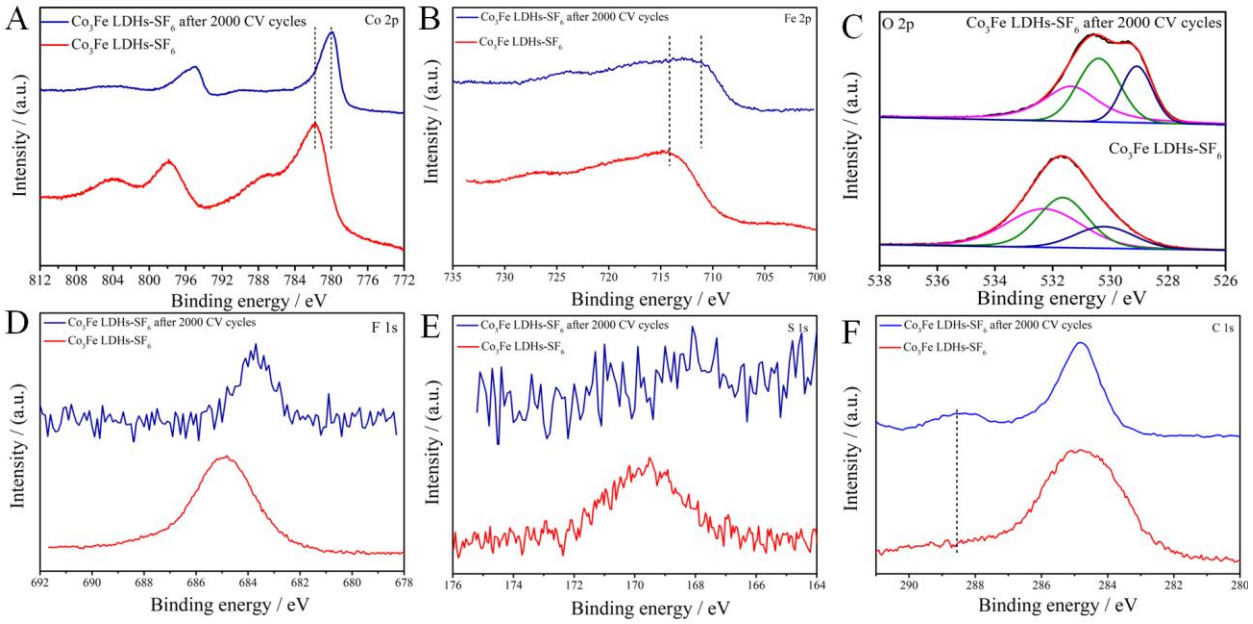

Figure 5. Co 2p (A), Fe 2p (B), O 1s (C), F 1s (D), S 2p (E) and C 1s (F) of Co_3Fe LDHs-SF_6 and Co_3Fe LDHs-SF_6 after 2000 CV cycles.

CONCLUSION

In summary, quinary Co_3Fe LDHs-SF_6 ultrathin nanosheets have been sucessfully synthesized by one step SF_6-plasma etching technique at room temperature. With SF_6-plasma treatment, interlamellar carbonate species can be removed to achieve exfoliation and LDHs surface can be etched to create oxygen vacanies and metal vacanies. What's more, part oxygen vacanies can be *in-situ* filled with S and F in ionized SF_6-plasma environment. With the increased number of active sites and modulated electronic structure, Co_3Fe LDHs-SF_6 only demands 268 mV to reach 10 mA cm^{-2}, which is more outstanding than some reported highly active OER electrocatalysts. Post characterization of Co_3Fe LDHs-SF_6 after stability test indicates a metal hydroxide layer can be formed at surface and worked as active sites. This work provides a simple method to achieve multielement co-doping by one step at room temperature and a novel strategy to

modulate electronic structure by incorpation of anions with different property. This work also demonstrates the relationship between electronic structure and electrochemical activity.

MATERIALS AND METHODS

Synthesis of Co_3Fe LDHs

Pristine Co_3Fe LDHs were synthesized in a hydrothermal method. First, solution A was formed by dissolving 0.9 mol $Co(NO_3)_2{\cdot}6H_2O$ and 0.3 mol $Fe(NO_3)_3{\cdot}9H_2O$ into 30 mL deionized water. The feeding rate of Co^{2+}/Fe^{3+} is 3:1. Solution B was formed by dissolving 1.92 mol NaOH and 0.8 mol Na_2CO_3 into 30 mL deionized water. Solution B was poured into solution A under intense stir for 30 min. Then obtained mixed solution was transferred into 100 mL Teflon-lined autoclave and heated at 80 ℃ for 48 h. After cooling down to room temperature, pristine Co_3Fe LDHs were obtained by washing with deionized water and ethanol and then dried at 60 ℃ under vacuum condition.

Synthesis of Co_3Fe LDHs-SF_6

Co_3Fe LDHs-SF_6 was prepared by a SF_6-plasma etching technique. Firstly, an ink was prepared by dispersing 20 mg Co_3Fe LDHs into 2 mL ethanol under ultrasound. Then 1500 μL ink was dropped into a 4 cm*4 cm clean Ti foil and dried naturally at room temperature. Afterwards, put Ti foil into MARCH plasma reactor and treated by SF_6-plasma with a power of 10 W for 5 s, 20 s, 80 s and 120 s. The flow rate was 3 sccm. The powder was stripped from Ti foil with blade. Pristine Co_3Fe LDHs that treated by SF_6-plasma for 80 s was explored in detail.

Physical characterization

SEM (JEOL 7600F) and TEM (JEOL 2100F; FEI Talos 200x) were used to explore the morphology and crystalline phase structure of LDHs nanosheets. AFM (Brucker Bioscope system) was used to explore the size and thickness of LDHs nanosheets. XRD (Bruker D8 Advance diffractometer, Cu Kα1) was used to explore the structure of LDHs nanosheets. EXAFS and XANES were carried out to explore coordination configuration and electronic environment of LDHs nanosheets at BL17C at National Synchrotron Radiation Research Center, Taiwan. BET analysis was performed on JW-BK200C and XPS was analyzed with Al-Kα X-ray ($h\nu = 1486.6$ eV) radiation (Thermo Fisher Scientific, England). Elemental concentrations (Fe and Co) within the solutions were determined by the ICP-OES analysis with an iCAP 6300 radial view inductively coupled plasma-optical emission spectrometer.

Electrocatalytic activity test

Electrocatalytic activity was evaluated in a three-electrode system using CHI 660 electrochemical workstation. Carbon rode and saturated calomel electrode (SCE) were worked as counter electrode and the reference electrode, respectively. Ink was prepared by dispersing 4 mg electrocatalyst into 500 μL deionized water, 500 μL ethanol and 50 μL 5 wt% Nafion under ultrasound for 30 min. Then, 10 μL ink was dropped on glassy carbon electrode (diameter: 5 mm), which was used as working electrode. The electrolyte solution is 1.0 M KOH. All Potentials were referenced to a reversible hydrogen electrode (RHE): $E_{RHE} = E_{SCE} + 0.242 + 0.059*pH$. Linear-sweep voltammetry (LSV) polarization curves were recorded at scan rate of 5 mV s^{-1}. Nyquist plots were measured in the frequency range between 0.01 Hz and 1000 kHz at 1.51 V (vs. RHE). Tafel slope was calculated according to equation: $\eta=b*\log(j) + a$, where η, b and j represent overpotential, Tafel slope and current density, respectively.

Author information

Corresponding authors

Yanyong Wang, Email: yanyongwang@hnu.edu.cn.

Chung-Li Dong, Email: cldong@mail.tku.edu.tw.

Shuangyin Wang, Email: shuangyinwang@hnu.edu.cn.

Acknowledgements

This work was supported by Hunan Provincial Innovation Foundation for Postgraduate (Grant No. CX2018B181) and National Natural Science Foundation of China (Grant No: 21573066, 21825201 and 2187350). This research used resources of the Center for Functional Nanomaterials, which is a U.S. DOE Office of Science Facility, at Brookhaven National Laboratory under Contract No. DE-SC0012704.

Competing interests: The authors declare that they have no competing interests. Data and materials availability: All data needed to evaluate the conclusions in the paper are present in the paper and/or the Supplementary Materials. Additional data related to this paper may be requested from the corresponding authors.

REFERENCES AND NOTES.

1. Lee, J.-S.; Tai Kim, S.; Cao, R.; Choi, N.-S.; Liu, M.; Lee, K. T.; Cho, J., Metal–Air Batteries with High Energy Density: Li–Air versus Zn–Air. *Advanced Energy Materials* **2011,** *1* (1), 34-50.

2. Joya, K. S.; Joya, Y. F.; Ocakoglu, K.; van de Krol, R., Water-Splitting Catalysis and Solar Fuel Devices: Artificial Leaves on the Move. *Angewandte Chemie International Edition* **2013,** *52* (40), 10426-10437.

3. Gao, K.; Wang, B.; Tao, L.; Cunning, B. V.; Zhang, Z.; Wang, S.; Ruoff, R. S.; Qu, L., Efficient Metal-Free Electrocatalysts from N-Doped Carbon Nanomaterials: Mono-Doping and Co-Doping. *Advanced Materials* **2019,** *31* (13), 1805121.

4. Wang, Y.; Yan, D.; El Hankari, S.; Zou, Y.; Wang, S., Recent Progress on Layered Double Hydroxides and Their Derivatives for Electrocatalytic Water Splitting. *Advanced Science* **2018,** *5* (8), 1800064.

5. Wang, H. F.; Tang, C.; Li, B. Q.; Zhang, Q., A review of anion regulated multi-anion transition metal compounds for oxygen evolution electrocatalysis. *Inorganic Chemistry Frontiers* **2018,** *5* (3), 521-534.

6. Li, B. Q.; Zhang, S. Y.; Tang, C.; Cui, X.; Zhang, Q., Anionic Regulated NiFe (Oxy)Sulfide Electrocatalysts for Water Oxidation. *Small* **2017,** *13* (25), 1700610.

7. Liu, Z.; Wang, Y.; Chen, R.; Chen, C.; Yang, H.; Ma, J.; Li, Y.; Wang, S., Quaternary bimetallic phosphosulphide nanosheets derived from prussian blue analogues: Origin of the ultra-high activity for oxygen evolution. *Journal of Power Sources* **2018,** *403*, 90-96.

8. Han, L.; Yu, X.-Y.; Lou, X. W., Formation of Prussian-Blue-Analog Nanocages via a Direct Etching Method and their Conversion into Ni–Co-Mixed Oxide for Enhanced Oxygen Evolution. *Advanced Materials* **2016,** *28* (23), 4601-4605.

9. Qian, J.; Guo, X.; Wang, T.; Liu, P.; Zhang, H.; Gao, D., Bifunctional porous Co-doped NiO nanoflowers electrocatalysts for rechargeable zinc-air batteries. *Applied Catalysis B: Environmental* **2019,** *250*, 71-77.

10. Yang, H.; Hu, Y.; Huang, D.; Xiong, T.; Li, M.; Balogun, M. S.; Tong, Y., Efficient hydrogen and oxygen evolution electrocatalysis by cobalt and phosphorus dual-doped vanadium nitride nanowires. *Materials Today Chemistry* **2019,** *11*, 1-7.

11. Song, F.; Hu, X., Exfoliation of layered double hydroxides for enhanced oxygen evolution catalysis. *Nature Communications* **2014,** *5*, 4477.

12. Shui, J.; Wang, M.; Du, F.; Dai, L., N-doped carbon nanomaterials are durable catalysts for oxygen reduction reaction in acidic fuel cells. *Science Advances* **2015,** *1* (1), e1400129-e1400129.

13. Kuanping, G.; Feng, D.; Zhenhai, X.; Michael, D.; Liming, D., Nitrogen-doped carbon nanotube arrays with high electrocatalytic activity for oxygen reduction. *Science* **2009,** *323* (5915), 760-764.

14. Hyuck, C. C.; Sung Hyeon, P.; Seong Ihl, W., Binary and ternary doping of nitrogen, boron, and phosphorus into carbon for enhancing electrochemical oxygen reduction activity. *Acs Nano* **2012,** *6* (8), 7084-7091.

15. Wang, H. Y.; Hung, S. F.; Chen, H. Y.; Chan, T. S.; Chen, H. M.; Liu, B., In Operando Identification of Geometrical-Site-Dependent Water Oxidation Activity of Spinel Co3O4. *Journal of the American Chemical Society* **2015,** *138* (1), 36-39.

16. Wang, Y.; Qiao, M.; Li, Y.; Wang, S., Tuning Surface Electronic Configuration of NiFe LDHs Nanosheets by Introducing Cation Vacancies (Fe or Ni) as Highly Efficient Electrocatalysts for Oxygen Evolution Reaction. *Small* **2018,** *14* (17), 1800136.

17. Chen, L.; Chang, J.; Zhang, Y.; Gao, Z.; Wu, D.; Xu, F.; Guo, Y.; Jiang, K., Fluorine anion-enriched nickel hydroxyl oxide as an efficient oxygen evolution reaction electrocatalyst. *Chemical Communications* **2019,** *55*, 3406-3409.

18. Zhu, Y.; Zhou, W.; Ran, R.; Chen, Y.; Shao, Z.; Liu, M., Enhancing electrocatalytic activity of perovskite oxides by tuning cation deficiency for oxygen reduction and evolution reactions. *Chemistry of Materials* **2016,** *28* (6), 1691-1697.

19. Zhuang, L.; Ge, L.; Yang, Y.; Li, M.; Jia, Y.; Yao, X.; Zhu, Z., Ultrathin Iron-Cobalt Oxide Nanosheets with Abundant Oxygen Vacancies for the Oxygen Evolution Reaction. *Advanced Materials* **2017,** *29* (17), 1606793.

20. Qiang, F.; Wei-Xue, L.; Yunxi, Y.; Hongyang, L.; Hai-Yan, S.; Ding, M.; Xiang-Kui, G.; Limin, C.; Zhen, W.; Hui, Z., Interface-confined ferrous centers for catalytic oxidation. *Science* **2010,** *328* (5982), 1141-1144.

21. Liu, Z.; Dong, C.-L.; Huang, Y.-C.; Cen, J.; Yang, H.; Chen, X.; Tong, X.; Su, D.; Wang, Y.; Wang, S. Modulating the electronic structure of ultrathin layered double hydroxide nanosheets with fluorine: an efficient electrocatalyst for the oxygen evolution reaction. *Journal of Materials Chemistry A* **2019,** *7* (24), 14483-14488.

22. Ren, J.; Ouyang, S.; Xu, H.; Meng, X.; Wang, T.; Wang, D.; Ye, J., Targeting Activation of CO2 and H2 over Ru-Loaded Ultrathin Layered Double Hydroxides to Achieve Efficient Photothermal CO2 Methanation in Flow-Type System. *Advanced Energy Materials* **2017,** *7* (5), 1601657.

23. Liu, R.; Wang, Y.; Liu, D.; Zou, Y.; Wang, S., Water-Plasma-Enabled Exfoliation of Ultrathin Layered Double Hydroxide Nanosheets with Multivacancies for Water Oxidation. *Advanced Materials* **2017,** *29* (30), 1701546.

24. Wang, Y.; Zhang, Y.; Liu, Z.; Xie, C.; Feng, S.; Liu, D.; Shao, M.; Wang, S., Layered Double Hydroxide Nanosheets with Multiple Vacancies Obtained by Dry Exfoliation as Highly

Efficient Oxygen Evolution Electrocatalysts. *Angewandte Chemie International Edition* **2017,** *56* (21), 5867-5871.

25. Pei, C.; Chen, H.; Dong, B.; Yu, X.; Feng, L., Electrochemical oxygen evolution reaction efficiently catalyzed by a novel porous iron-cobalt-fluoride nanocube easily derived from 3-dimensional Prussian blue analogue. *Journal of Power Sources* **2019,** *424*, 131-137.

26. Ouyang, C.; Wang, X.; Wang, S., Phosphorus-doped CoS2 nanosheet arrays as ultra-efficient electrocatalysts for the hydrogen evolution reaction. *Chemical Communications* **2015,** *51* (75), 14160-14163.

27. Bora, D. K.; Cheng, X.; Kapilaschrami, M.; Glans, P. A.; Luo, Y.; Guo, J., Influence of crystal structure, ligand environment and morphology on Co L – edge XAS spectral characteristics in cobalt compounds. *Journal of Synchrotron Radiation* **2015,** *22* (6), 1450–1458.

28. Zhang, Y.; Lin, Y.; Jiang, H.; Wu, C.; Liu, H.; Wang, C.; Chen, S.; Duan, T.; Song, L., Well-Defined Cobalt Catalyst with N-Doped Carbon Layers Enwrapping: The Correlation between Surface Atomic Structure and Electrocatalytic Property. *Small* **2018,** *14* (6), 1702074.

29. Tian, C.; Xu, Y.; Nordlund, D.; Lin, F.; Liu, J.; Sun, Z.; Liu, Y.; Doeff, M., Charge Heterogeneity and Surface Chemistry in Polycrystalline Cathode Materials. *Joule* **2018,** *2* (3), 464-477.

30. Shen, S.; Zhou, J.; Dong, C.-L.; Hu, Y.; Tseng, E. N.; Guo, P.; Guo, L.; Mao, S. S., Surface Engineered Doping of Hematite Nanorod Arrays for Improved Photoelectrochemical Water Splitting. *Scientific Reports* **2014,** *4*, 6627.

31. Nemrava, S.; Vinnik, D. A.; Hu, Z.; Valldor, M.; Kuo, C.-Y.; Zherebtsov, D. A.; Gudkova, S. A.; Chen, C.-T.; Tjeng, L. H.; Niewa, R., Three Oxidation States of Manganese in the Barium Hexaferrite BaFe12–xMnxO19. *Inorganic Chemistry* **2017,** *56* (7), 3861-3866.

32. Oishi, M.; Yamanaka, K.; Watanabe, I.; Shimoda, K.; Matsunaga, T.; Arai, H.; Ukyo, Y.; Uchimoto, Y.; Ogumi, Z.; Ohta, T., Direct observation of reversible oxygen anion redox reaction in Li-rich manganese oxide, Li2MnO3, studied by soft X-ray absorption spectroscopy. *Journal of Materials Chemistry A* **2016,** *4* (23), 9293-9302.

33. Wang, S.; Yao, M.; Li, Z.; Feng, C.; Wang, L.; Tang, X.; Kang, P.; Zhang, B.; Mi, W.; Yu, G., Nitrogen Tuned Charge Redistribution and Orbital Reconfiguration in Fe/MgO Interface for Significant Interfacial Magnetism Tunability. *Advanced Functional Materials* **2019,** *29* (4), 1806677.

34. Baker, M. L.; Mara, M. W.; Yan, J. J.; Hodgson, K. O.; Hedman, B.; Solomon, E. I., K- and L-edge X-ray absorption spectroscopy (XAS) and resonant inelastic X-ray scattering (RIXS) determination of differential orbital covalency (DOC) of transition metal sites. *Coordination Chemistry Reviews* **2017,** *345*, 182-208.

35. Li, Z.; Duan, H.; Shao, M.; Li, J.; O'Hare, D.; Wei, M.; Wang, Z. L., Ordered-Vacancy-Induced Cation Intercalation into Layered Double Hydroxides: A General Approach for High-Performance Supercapacitors. *Chem* **2018,** *4* (9), 2168-2179.

36. Xu, L.; Jiang, Q.; Xiao, Z.; Li, X.; Huo, J.; Wang, S.; Dai, L., Plasma-Engraved Co3O4 Nanosheets with Oxygen Vacancies and High Surface Area for the Oxygen Evolution Reaction. *Angewandte Chemie International Edition* **2016,** *55* (17), 5277-5281.

37. Wang, S.; Xiao, Z.; Wang, Y.; Huang, Y. C.; Wei, Z.; Dong, C. L.; Ma, J.; Shen, S.; Li, Y., Filling the Oxygen Vacancies in Co3O4 with Phosphorus: an Ultra-efficient Electrocatalyst for the Overall Water Splitting. *Energy & Environmental Science* **2017,** *10* (12), 2563-2569.

38. Youwen, L.; Chong, X.; Mengjie, L.; Yue, L.; Weizheng, C.; Pengcheng, H.; Wei, T.; Youming, Z.; Yi, X., Ultrathin Co3S4 nanosheets that synergistically engineer spin states and

exposed polyhedra that promote water oxidation under neutral conditions. *Angew Chem Int Ed Engl* **2015,** *127* (38), 11383-11387.

39. Hussain, N.; Yang, W.; Dou, J.; Chen, Y.; Qian, Y.; Xu, L., Ultrathin mesoporous F-doped α-Ni(OH)2 nanosheets as an efficient electrode material for water splitting and supercapacitors. *Journal of Materials Chemistry A* **2019,** *7* (16), 9656-9664.

40. Yuan, Z.; Bak, S.-M.; Li, P.; Jia, Y.; Zheng, L.; Zhou, Y.; Bai, L.; Hu, E.; Yang, X.-Q.; Cai, Z.; Sun, Y.; Sun, X. Activating Layered Double Hydroxide with Multivacancies by Memory Effect for Energy-Efficient Hydrogen Production at Neutral pH. *ACS Energy Letters* **2019,** *4* (6), 1412-1418.

41. Hunter, B. M.; Hieringer, W.; Winkler, J. R.; Gray, H. B.; Müller, A. M., Effect of interlayer anions on [NiFe]-LDH nanosheet water oxidation activity. *Energy & Environmental Science* **2016,** *9* (5), 1734-1743.
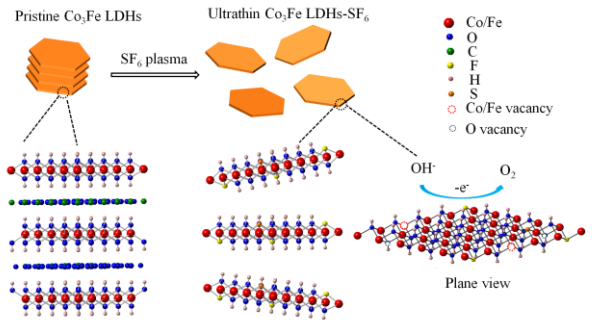
TOC